Terahertz seventeen-band metamaterial absorber based on sunflower-typed structure

A. ELAKKIYA[1*], K. A. KARTHIGEYAN[2], E. MANIKANDAN[3], S. RADHA[2]
[1]*Department of ECE, Saveetha Engineering College, Chennai – 602105, India*
[2]*Department of ECE, Sri Sivasubramaniya Nadar College of Engineering, Chennai – 603110, India*
[3]*School of Electronics Engineering, Vellore Institute of Technology, Chennai Campus – 600127, India*

Terahertz (THz) Metamaterial Absorbers (MMAs) have gained attention for applications like imaging, sensing and spectroscopy. In specific, there is a need for designing a multi-band MMA. In this study, a new MMA is proposed and designed to operate at seventeen distinct frequencies using a single resonator concept. It is designed to achieve a bandwidth of 440 GHz in the range (750-1190 GHz). By optimizing the top metallic patch geometrical parameter (r2) eleven-/fourteen-/fifteen-/sixteen-band MMAs have been obtained. The proposed has stable response for various incident angles of up to 90^0 and also polarization independent characteristics. For understanding the underlying mechanism of multi-band operation the electric and magnetic field distributions are analysed. The proposed structure has achieved a sharp narrow-band absorption in the desired resonances. In terahertz regime, this is the first of kind to achieve seventeen-band absorber with better absorption characteristics using a simple planar structure. This kind of structure finds importance in sensing and imaging applications.

(Received January 10, 2022; accepted October 5, 2022)

Keywords: Seventeen-band MMA, Polarization and incident angle insensitive, Terahertz

1. Introduction

THz is a range of frequencies from 0.1-10 THz i.e. in-between microwave and infrared region [1]. Since the development of high power sources, it has involved widely in various applications such as sensing [2], medical imaging [3], public security [4], frequency-selective detection [5], next-generation communication [6], etc. For taking the advantages of this full band, it is necessary to construct a novel THz components, including absorbers, antennas, sensors, modulators, and filters [7-10]. Among these, absorber has gained more attention due to the usage in imaging, modulation, and sensing. But most of the MMAs have a single band absorption due to the structure of MM [11-15], which is not desirable for practical applications. For increasing the number of resonances, generally two design approaches have been used, stacking of planar structures vertically or unit-cell design with structures of different sizes [16-20]. But these two methods can obtain six-/five-/triple-band absorption and also the complexity increases. These absorbers have certain drawbacks: complicated fabrication process, multilayer complexed structures, and larger unit-cell size, which limit their use for real-time applications. It is really excited if a single resonator able to support higher order resonances in addition to the fundamental resonance.

Recently, group of researchers [21-24] have designed a multiband THz perfect absorbers. And maximum of eight resonances have been achieved, and the majority of the structures have achieved polarization-dependent characteristics also. Dan Hu *et* al. [25] have designed a fifteen-band THz MMA based on metal groove structure with high-k material substrate and the structure is complex in nature. Therefore, designing a simple structure for multi-band absorber application with polarization-insensitive characteristics is still a challenge one for the researcher. To insert new force into the field of multiple bands MMAs, we propose an ultra-multiband, polarization-sensitive THz absorber formed by a single planar structure with low-k material. Simulated results demonstrate that the projected absorber has seventeen distinct absorption bands in the (0.75-1.19) THz frequency range. We compared this ultra-multiband MMA with previous multi-band absorbers as shown in Table 1.

Table 1. Analysis of results comparisons with reported works in the literature

Ref.	Year	No. of. resonances	Developed Methods: Coplanar(C), Stacked(S)	Number of resonating elements	Materials
[26]	2016	1	C	4	Silver, glass
[27]	2011	2	C+S	2	Au, polyimide, Si
[28]	2012	3	C+S	3	Au, polyimide, Si
[29]	2015	4	C+S	2	Au, polyimide, Si
[30]	2020	5	C	3	Au, polyimide
[31]	2017	6	S	1	Au, polyimide, Si
[32]	2020	7	-	1	Cu, polyimide
[33]	2019	8	-	1	Au, GaAs
[25]	2020	15	C	25	Cu, GaAs
This work	-	17	-	1	Cu, polyimide

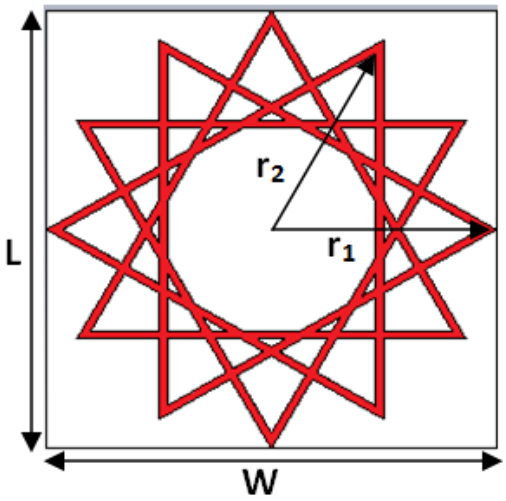

Fig. 1. Unit-cell design of the proposed MMA (W=L=500 μm, r_1=250 μm, r_2=232 μm, h=125 μm) (color online)

Compared to previous works [26-34], the proposed MMA has some distinct advantages: First, the MMA structure is novel, compact, simple, and provides an ultra-multiband within a narrowed range of (0.75 – 1.19) THz. Second, this metamaterial absorber can provide seventeen-band resonant characteristics using a single planar structure in terahertz regime; Third, by varying the top patch metallic geometrical parameter (r_2) eleven-/fourteen-/fifteen-/sixteen-band MMAs have been obtained. Finally, the structure has obtained polarization and incident angle independent nature which is confirmed in numerical evaluation. Unit-cell boundary condition is used at X and Y directions and open source boundary condition is applied at the Z direction. Commercially available CST Microwave Studio Software-2021 version is used to do a simulation works.

2. Materials and methods

Fig. 1 depicts the planned seventeen-band MA's structure. It is made up of a planar resonator structure separated by a low-dielectric-constant material with a thickness of 0.125 mm. Copper is used for the ground plane and top resonator, with a frequency-insensitive conductivity of $\sigma=5.8\times10^7$ S/m [36]. The substrate is made of polyimide, which has a loss factor (tan δ) of 0.0027 and a relative dielectric constant (ε_0) of 3.5. The ground plane and substrate material are both 0.5 mm wide (W) and long (L). The top patch resonator's inner (r2) and outer (r1) radius are 0.232 mm and 0.25 mm, respectively.

The study employs the unit-cell periodic boundary condition in the x and y directions, as well as the z open boundary condition. The simulation programme is used to obtain the absorption, reflection, and transmission parameters. Due to the presence of a thick metallic ground metal layer, which is larger than its skin depth (δ) value, the transmission spectra confirm zero transmission. As a result, only the reflection component determines absorption. Absorption is improved since the proposed structure has better reflections in the appropriate bands.

3. Results and discussions

The obtained absorption characteristics of the designed structure are shown in Fig. 2. In the simulated results, there are seventeen resonances seen at 0.75 THz

(f_1), 0.77 THz (f_2), 0.84 THz (f_3), 0.86 THz (f_4), 0.87 THz (f_5), 0.9 THz (f_6), 0.909 THz (f_7), 0.92 THz (f_8), 0.94 THz (f_9), 1 THz (f_{10}), 1.03 THz (f_{11}), 1.04 THz (f_{12}), 1.05 THz (f_{13}), 1.1 THz (f_{14}), 1.11 THz (f_{15}), 1.12 THz (f_{16}), and 1.17 THz (f_{17}) with absorptivity of 99.6 %, 98 %, 97 %, 73 %, 85 %, 96 %, 89 %, 83 %, 95 %, 70 %, 90 %, 85 %, 99 %, 95 %, 72 %, 92 % and 95 % respectively. The designed MMA's reflection properties (in dB) are illustrated in Fig. 3. In all of the desired resonances, the structure exhibits a return loss of less than 10dB, resulting in unity absorption characteristics.

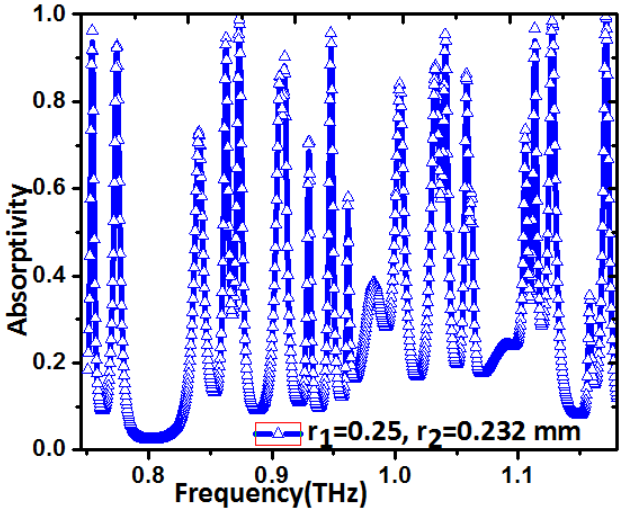

Fig.2. Obtained absorption characteristics of the designed seventeen-band MMA (color online)

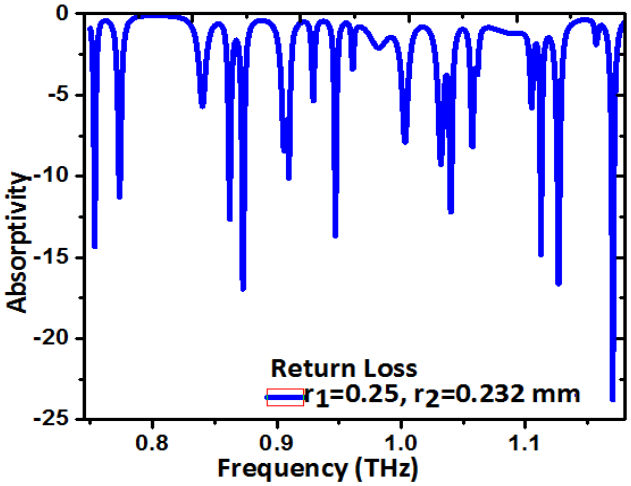

Fig. 3. Return loss of the proposed seventeen- band MMA (color online)

3.1. Polarization and angular stability

The proposed metamaterial absorber's simulated absorbance is illustrated in Fig. 4 (a) and (b), where the oblique incidence angle and polarisation angle are varied from 0 to 90^0 in the frequency range of interest (0.75 to 1.19 THz). The structure's absorption and resonant frequency did not change while the polarisation angle and incidence angle values were changed. As a result, the suggested MMA has exceptional polarization-independent absorption properties. This is primarily owing to the intended MMA's unit-cell symmetry.

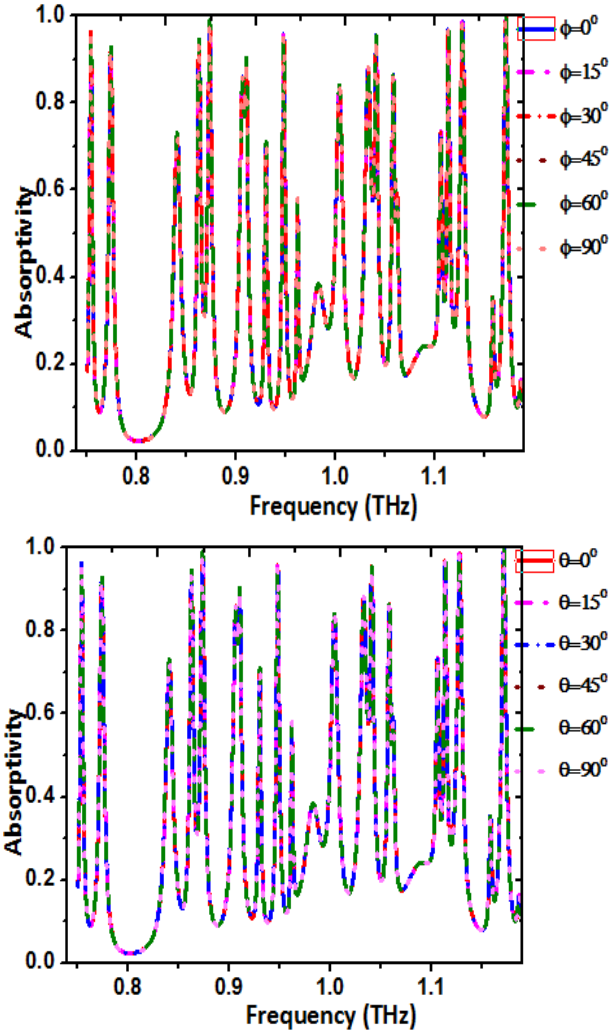

Fig. 4. Absorbance characteristics of the proposed structure for (a) different incident angle (b) different polarization angles under normal incidence condition (color online)

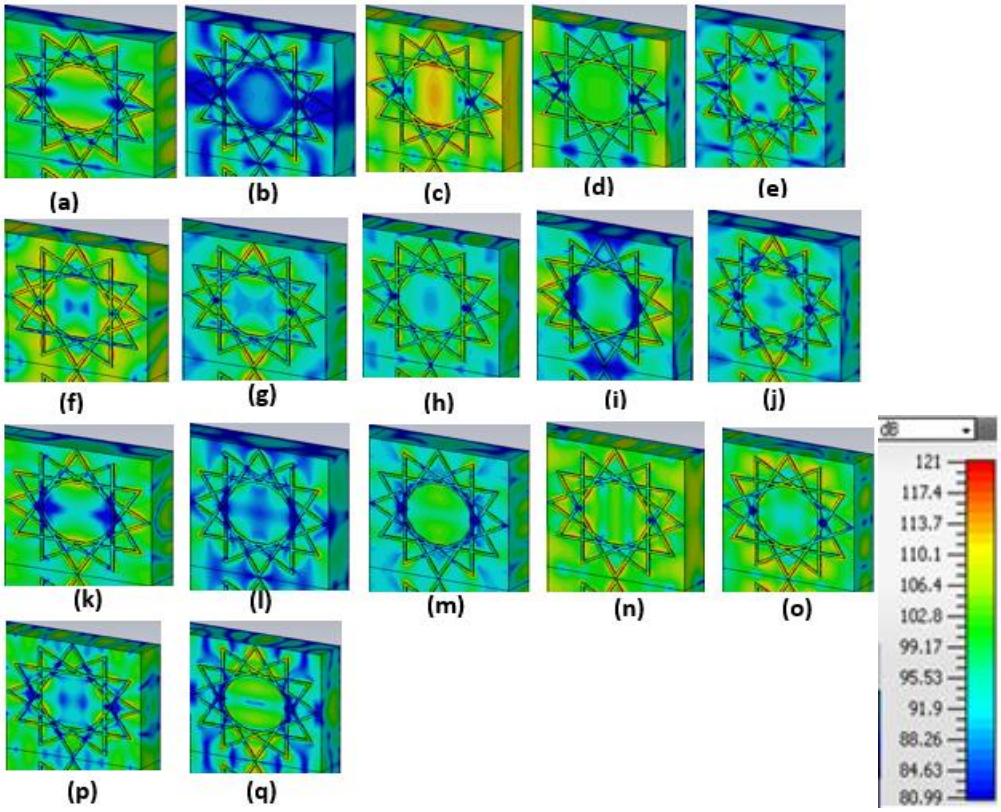

Fig. 5. Electric field distribution of seventeen-band absorber for the resonance frequencies of (a) 0.75 THz, (b) 0.77 THz, (c) 0.84 THz, (d) 0.86 THz, (e) 0.87 THz, (f) 0.9 THz, (g) 0.909 THz, (h) 0.92 THz, (i) 0.94 THz, (j) 1 THz, (k) 1.03 THz, (l) 1.04 THz, (m) 1.05 THz, (n) 1.1 THz, (o) 1.11 THz, (p) 1.12 THz, (q) 1.17 THz (color online)

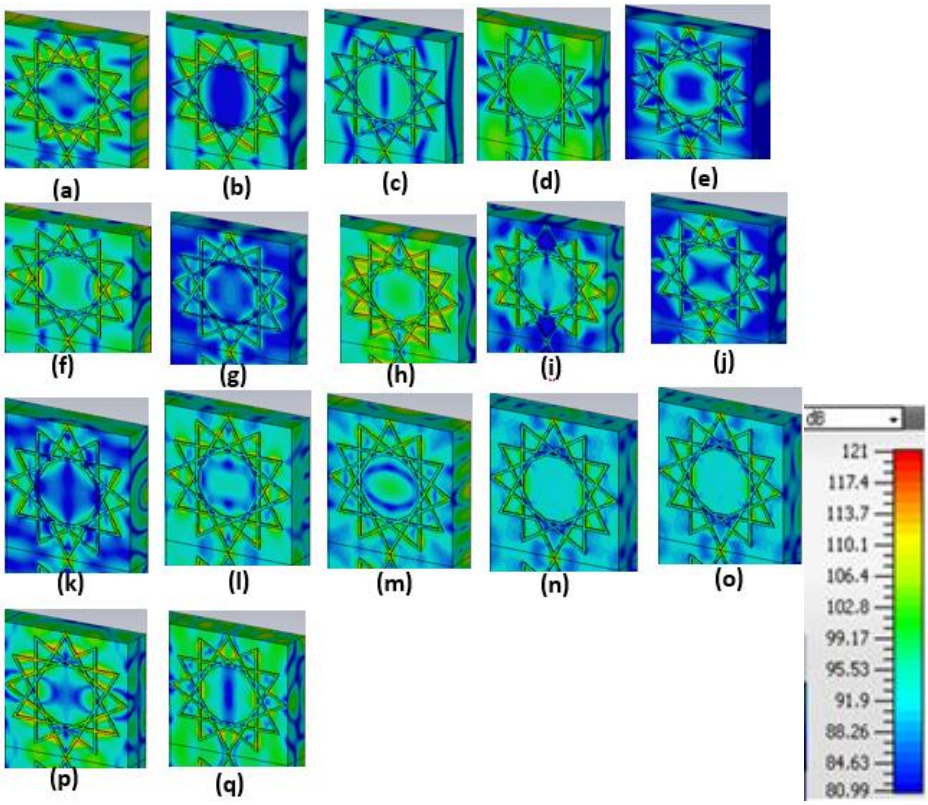

Fig. 6. Magnetic field distribution of seventeen-band absorber for the resonance frequencies of (a) 0.75 THz, (b) 0.77 THz, (c) 0.84 THz, (d) 0.86 THz, (e) 0.87 THz, (f) 0.9 THz, (g) 0.909 THz, (h) 0.92 THz, (i) 0.94 THz, (j) 1 THz, (k) 1.03 THz, (l) 1.04 THz, (m) 1.05 THz, (n) 1.1 THz, (o) 1.11 THz, (p) 1.12 THz, (q) 1.17 THz (color online)

3.2. Electric and magnetic field distributions (E-field& H-field)

Energy dissipation and absorption mechanisms are well-known to be strongly dependent on the electromagnetic (EM) field. The mechanism of absorption-based E-field and H-field at seventeen corresponding frequencies will be explored in this part. This MMA, as seen in Fig.5, has produced a high E-field (a-q). As illustrated in Fig.5 (a), (c), (f), (n), and (o), the patch resonator and dielectric layer do a great job of detaining the electric field (o). As demonstrated in Fig. 5 (b), (l), and (m), the E-field is greatest across the patch structure and in some locations on the dielectric surface (q). As illustrated in Fig. 5 (d), (e), (q), (g-k), (m), and (n), the entire patch resonator and the surface of the dielectric do an excellent job of confining the electric field (p).

The matching magnetic field distribution is utilised to analyse the process of absorption. Fig. 6 depicts the magnetic field's good containment (a-q). The absorption curve is focused everywhere over the resonant structure and in some areas on the dielectric surface, as shown in Fig.6 (e), (g), I (j), and (k). As illustrated in Fig.6 (a), (f), (d), (h), (p), and (q), the patch resonator and dielectric layer do a great job of detaining the magnetic field (q). As illustrated in Fig.6 (b), (c), (l), (m), (n), and (o), the M-field is greatest across the patch structure and on the dielectric surface (o).

3.3. Quality factor (Q)

The Q value (defined as the resonance frequency point divided by its Full-Width Half Maximum (FWHM)) is a popular criterion for determining whether or not to use the resonance mode. It may clearly state whether or not the frequency mode can be used for sensing. When the Q value is larger, the sensing performance is enhanced [35]. The Q value is calculated for all of the frequency points and summarised in Table 2 along with the explanation of the Q value. Except for the 5th and 11th frequency modes, all of the frequency modes have a Q value greater than 50. In comparison to other modes, the 14th mode has the highest Q-factor value. The design of the seventeen-band absorber is promising in sensor-related disciplines due to its high Q-factor.

Table 2. Q-factor and FWHM values for seventeen frequencies

Peaks	F (THz)	A (%)	FWHM	Q
1	0.75	99	0.00337	224
2	0.77	98	0.00591	131
3	0.84	97	0.00813	103
4	0.86	73	0.01	86
5	0.87	85	0.03	29
6	0.90	96	0.00947	96
7	0.90	89	0.00956	95
8	0.92	83	0.00319	291
9	0.94	95	0.0035	270
10	1	70	0.00656	152
11	1.03	90	0.02214	46
12	1.039	85	0.01	103
13	1.05	99	0.00685	154
14	1.105	95	0.0027	**409**
15	1.11	72	0.01978	56
16	1.12	92	0.00642	175
17	1.17	95	0.00536	218

3.4. Parametric analysis

Parameter studies aid in determining the appropriate absorbance value and structure use. Fig. 7 (a), (b), and (c) show the influence of the r2 on the absorption spectra when other geometric factors are maintained or unchanged (d).

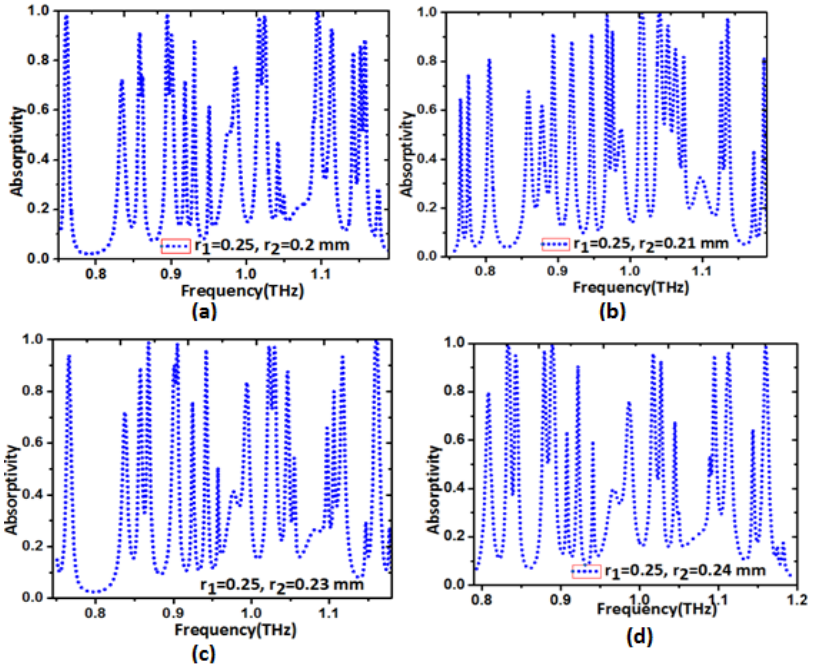

Fig. 7. (a-d). Absorption curve as a function of radius r_2 (color online)

The MMA resonated at fifteen, eleven, sixteen, fourteen, and seventeen different frequencies with maximum absorptivity when the r2 value was 0.2 mm, 0.21 mm, 0.23 mm, 0.24 mm, and 0.232 mm. Table 3 shows the resonant frequencies and absorption rates based on the r2 value. The geometric parameters of the unit-cell structure has a considerable impact on the resonance frequencies and absorption curves of the proposed seventeen-band metamaterial absorber.

Table 3. Number of resonant modes with respect to r_2

r_2(mm)	No. of peaks	Absorptivity (%)	Resonant Frequencies (THz)
0.2	15	95,98,85,99.9,98,94,78,98,97,99.9,94,81,83	0.75,0.78,0.88,0.91,0.94,0.96,0.97,1.03,1.04,1.05,1.07,1.13,1.14
0.21	15	81.7,99,92,84,85,95,99.9,99.9,97,99,93,90,96,82,80	0.753,0.78,0.88,0.91,0.94,0.96,0.97,1,1.03,1.04,1.05,1.07,1.12,1.13,1.19
0.23	16	99.9,93,79,88,97,97,83,96,76,98,90,99,89,72,94,91	0.75,0.76,0.85,0.86,0.87,0.9,0.91,0.93,0.94,1,1.03,1.037,1.05,1.11,1.12,1.17
0.24	14	96,95,94,92,95,75,90,99.8,97,95,99,80,99.8,99.8	0.75,0.76,0.83,0.85,0.86,0.9,0.907,0.937,0.99,1.02,1.03,1.1,1.12,1.16
0.232	17	99.6 ,98,97,73,85,96,89,83,95,70,90,85,99,95,72,92,95	0.75,0.77,0.84,0.86,0.87,0.9,0.909,0.92,0.94,1,1.03,1.04,1.05,1.1,1.11,1.12,1.17

4. Conclusion

A novel MMA has been reported in this study at seventeen different frequencies without the need of stacked layers or numerous resonators. Eleven/thirteen/fourteen/sixteen-band MMAs have been generated by modifying the single top patch geometrical parameter. It has a wide frequency range of 440 GHz (750-1190 GHz). The proposed structure works well for incidence angles up to 900 degrees and polarisation angles up to 900 degrees. Electric and magnetic field distributions are used to investigate the structure's physical mechanism. In this study, we compared the resonant frequency ranges and number of bands to those reported in earlier studies. The Q-factor is used to investigate this MMA's sensing characteristics. values. In terahertz range, this is the first time a single planar structure provides seventeen-band high-level absorption performances. This will be used for material sensing, optoelectronics, terahertz imaging.

References

[1] M. Tonouchi, Nat Photonics **1**, 97 (2007).
[2] Haijun Zou, Yongzhi Cheng, Opt. Mater. **88**, 674 (2019).
[3] S. A. Kuznetsov, A. G. Paulish, A. V. Gelfand, P. A. Lazorskiy, V. N. Fedorinin, Progress in Electromagnetics Research **122**, 93 (2012).
[4] Li Huang, Dibakar Roy Chowdhury, Suchitra Ramani, Matthew T. Reiten, Sheng-Nian Luo, Antoinette J. Taylor, Hou-Tong Chen, Opt. Lett. **37**, 154 (2012).
[5] B. X. Wang, X. Zhai, G. Z. Wang, W. Q. Huang, L. L. Wang, IEEE Photonics J. **7**, 1 (2015).
[6] Runmei Gao, Zongcheng Xu, Chunfeng Ding, Liang Wu, Jianquan Yao, Opt. Commun. **356**, 400 (2015).
[7] A. T. Devapriya, S. J, Robinson, Microw. Optoelectron. Electromagn. Appl. **18**, 377 (2019).
[8] Zhou Hao, Ding Fei, Jin Yi, S. He, Prog. Electromagn. Res. **119**, 449 (2011).
[9] Jianjun Liu, Zhi Hong, Opt. Commun. **1**, 598 (2018).
[10] Hu Tao, Nathan Landy, Chris Bingham, Xin Zhang, Richard Averitt, Willie Padilla, Opt. Express **16**, 7181 (2008).
[11] B. Wang, C. Tang, Q. Niu, Y. He, Toe, Nanoscale Res. Lett. **14**, 64 (2019).
[12] Limei Qi, Chang Liu, Syed Mohsin Ali Shah, Carbon **153**, 179 (2019).
[13] F. Chen, Y. Cheng, H. A. Luo, Materials **13**, 860 (2020).
[14] Tran Van Huynh, Bui Son Tung, Bui Xuan Khuyen, Son Tung Ngo, Vu Dinh Lam, Comput. Mater. Sci. **166**, 276 (2019).
[15] Huiliang Ou, Fangyuan Lu, Yuhang Liao, Fengdi Zhu, Yu-Sheng Lin, Results Phys. **16**, 102897 (2020).
[16] Dong Wang, Yeqing Zhu, Cheng Fang, Ping He, Yonghong Ye, Appl. Opt. **58**, 7035 (2019).
[17] Ben-Xin Wang, Qin Xie, Guangxi Dong, Wei-Qing Huang, J. Electron. Mater. **48**,

2209 (2019).
[18] Yi Luo, Dejia Meng, Zhongzhu Liang, Jin Tao, Jingqiu Liang, Changhong Chen, Jianjun Lai, Tarik Bourouina, Yuxin Qin, Jinguang Lv, Yuhao Zhang, Opt. Commun. **459**, 124948 (2020).
[19] H. Luo, H. Hu, Y. Qiu, P. Zhou, Solid State Commun. **188**, 5 (2014).
[20] Govind Dayal, S. Ramakrishna, J. Opt. **15**, 5 (2013).
[21] H. Y. Meng, L. L. Wang, X. Zhai, G. D. Liu, S. X. Xia, Plasmonics **13**, 269 (2018).
[22] V. K. Verma, S. K. Mishra, K. K. Kaushal, V. Lekshmi, S. Sudhakar, S. K. Mishra, B. Appasani, N. Gupta, Plasmonics **15**, 75 (2020).
[23] B. X. Wang, G. Z. Wang, Appl. Phys. Express **10**, 03430 (2017).
[24] D. Hu, H. Y. Wang, Q. F. Zhu, IEEE Photon. J. **8**, 5500608 (2016).
[25] Dan Hu, Hongyan Wang, Jinfeng Zhang, Zhi Wang, Xiwei Zhangand Qiaofen Zhu, J. Phys. D Appl. Phys. **53**, 27 (2020).
[26] Z. Yong, S. Zhang, C. Gong, S. He, Sci. Rep. **6**, 24063 (2016).
[27] Y. Ma, Q. Chen, J. Grant, S. C. Saha, A. Khalid, D. R. S. Cumming, Opt. Lett. **36**, 945 (2011).
[28] X. Shen, Y. Yang, Y. Zang, J. Gu, J. Han, W. Zhang, T. J. Cui, Appl. Phys. Lett. **101**, 154102 (2012).
[29] S. Liu, J. Zhuge, S. Ma, H. Chen, D. Bao, Q. He, L. Zhou, T. J. Cui, Appl. Phys. **118**, 245304 (2015).
[30] Ben-Xin Wang, Yuanhao He, Pengcheng Lou, Wei-Qing Huang, Fuwei Pi, Results in Phyics **16**, 102930 (2020).
[31] B. Wang, G. Wang, T. Sang, L. L. Wang, Sci. Rep. **7**, 41373 (2017).
[32] A. Elakkiya, Radha Sankararajan, B. S. Sreeja **47**, 400 (2020).
[33] Ben-Xin Wang, Wei Xu, Yangkuan Wu, Zhuchuang Yang, Shengxiong Lai, Liming Lu, Nanoscale Advances **4**, 1359 (2022).
[33] Ben-Xin Wang, Wei Xu, Yangkuan Wu, Zhuchuang Yang, Shengxiong Lai, Liming Lu, Nanoscale Advances **3**, 455 (2021).
[34] Ben-Xin Wang, Yuanhao He, Pengcheng Lou, Wenhui Xing, Nanoscale Advances **2**, 763 (2020).
[35] Ben-Xin Wang, Chongyang Xu, Guiyuan Duan, Jieying Jiang, Wei Xu, Zhuchuang Yang, Yangkuan Wu, Nanoscale Research Letters **17**, 35 (2022).

*Corresponding author: elakkiyakapil@gmail.com